Quantum Transport Simulations of Phosphorene Nanoribbon MOSFETs: Effects of Metal Contacts, Ballisticity and Series Resistance

Mirko Poljak* and Mislav Matić
Computational Nanoelectronics Group, Micro and Nano Electronics Laboratory
Faculty of Electrical Engineering and Computing, University of Zagreb, Zagreb, Croatia
*E-mail: mirko.poljak@fer.hr

***Abstract*—Performance of phosphorene nanoribbon (PNR) MOSFETs at "3 nm" logic technology node is studied using atomistic quantum transport simulations, with an emphasis on the impact of metal contacts, series resistance and transport ballisticity. We find that realistic metal contacts decrease drain current by up to 70%, which corresponds to more than 1400 Ωμm in contact resistance (R_{SD}). On the other hand, setting R_{SD} to 270 Ωμm, as foreseen by the International Roadmap for Devices and Systems (IRDS), PNR MOSFETs would need to operate at 50% to 70% of their ballistic limit, depending on PNR width, in order to meet IRDS targets.**

Keywords—ballisticity, FET, metal contacts, nanoribbon, NEGF, phosphorene, series resistance, quantum transport

I. Introduction

Phosphorene is a promising 2D material as an alternative to graphene or transition metal dichalcogenides for end-of-roadmap logic devices due to its layered structure, acceptable bandgap, appropriate carrier effective masses and mobility, and a higher immunity to crystal defects than e.g. graphene [1]–[5]. Large-area phosphorene MOSFETs have been reported experimentally, demonstrating promising performance and contact resistance values [6]–[8]. In terms of modeling and simulation, phosphorene MOSFETs have been studied mostly in the ballistic limit, whereas in cases where dissipative transport is covered the contacts have been assumed to be ideal i.e. having identical structure as the channel [3], [9], [10]. Quantum confinement by width engineering in phosphorene nanoribbons (PNRs) provides an additional way of tuning the electronic and transport features relevant for logic FET applications, such as the bandgap and charge carrier effective masses [2], [4], [11], [12]. In this work, we investigate the performance of PNR MOSFETs using atomistic quantum transport modeling and simulations coupled with top-of-the-barrier (ToB) model. We study the impact of metal contacts, parasitic series resistance, transport ballisticity and PNR width scaling on several FET figures-of-merit (FOMs), and find conditions under which PNR FETs could fulfill industry requirements at the "3 nm" logic CMOS technology node.

II. Methodology

The 15 nm-long nanoribbon Hamiltonians are expressed in an atomistic tight-binding (TB) basis [13]. Quantum transport based on non-equilibrium Green's function (NEGF) formalism is employed to find geometry-dependent material properties such as density of states (DOS) and transmission. In terms of source/drain (S/D) contacts attached to the channel within NEGF simulations we study two cases. First, ideal contacts assume that S/D contact regions are semi-infinite semiconducting PNRs identical to the channel, and here the surface Green's functions (SGFs) are solved by the Sancho-Rubio method [14]. Second, metal contacts are modeled using the wide-band limit (WBL) approximation in which we set the contact-channel coupling strength to $t = 3$ eV and metal DOS at the Fermi level of $g(E = E_F) = 0.2$ eV^{-1} (while we do not assume any specific metal and ignore possible Schottky barriers, the metal DOS value corresponds to that of Au(111) [15]). The WBL replaces iterative procedures for calculating the SGFs, and these two parameters (t and $g(E = E_F)$) lead to constant imaginary elements in the surface Green's function of metal contacts equal to $\Sigma^R_{S/D} = -0.9$i eV.

Ballistic current-voltage (I-V) characteristics are obtained using top-of-the-barrier (ToB) model that self-consistently solves electrostatics, i.e. Poisson equation, coupled to DOS and quantum transmission results from NEGF [16], [17]. Since transport is ballistic, the drain current is found from the Landauer formula, after self-consistence is achieved for ToB potential and electron density. A major drawback of the ToB model is that tunneling is not included, which makes it reliable for predicting FET performance only for gate lengths above approximately 15 nm where direct S-D tunneling should be negligible given the phosphorene effective masses [16]. In addition, bandgap values for the examined PNRs are larger than ≈1.5 eV, which should be high enough to suppress band-to-band tunneling (BTBT) at 0.7 V supply voltage (V_{DD}).

For our 15 nm-long PNR MOSFETs we analyze the impact of nanoribbon width (W) scaling in the ≈0.5 nm to ≈5.5 nm range, assume a gate oxide with equivalent oxide thickness (EOT) of 1 nm, undoped channel, and S/D doping of $m = 0.001$, where m is the molar fraction of areal density of phosphorus atoms. Quasi-Fermi levels in S/D regions are determined to maintain charge neutrality. In order to set the threshold voltage (V_{th}) as projected in the International Roadmap for Devices and Systems (IRDS) at "3 nm" logic node (N3) [18] and provide meaningful results, we set a significantly tighter requirement for the OFF-state current (I_{OFF}) equal to 0.87 nA/μm for all devices in this work. The IRDS sets this value at 10 nA/μm, however, ToB model results in perfect subthreshold slope (SS) of 60 mV/dec in all cases, whereas the projected SS in IRDS at N3 equals 82 mV/dec.

This work was sponsored by the Croatian Science Foundation (HRZZ) under the project CONAN2D (UIP-2019-04-3493).

III. Results and Discussion

Transfer characteristics reported in Fig. 1 show normal FET operation with V_{th} of about 0.25 V. In case of ideal contacts (Fig. 1a), maximum achievable normalized drain current (ON-state current, I_{ON}) is 1.85 mA/µm. We note that *I-V* curves are closely spaced, indicating a weak modification of the normalized I_{ON} with nanoribbon width. However, drain current is significantly lower in PNR FETs with metal contacts (Fig. 1b), reaching up to 0.52 mA/µm, i.e. 28% of the maximum obtained for ideal contacts. In this case the *I-V* characteristics are again matched except for the narrowest PNR with $W = 0.49$ nm that exhibits significantly lower I_{ON}.

Influence of nanoribbon width scaling on I_{ON}, shown in Fig. 2, reveals a monotonic decrease of the absolute I_{ON} (Fig. 2a) and a non-monotonic behavior of the width-normalized I_{ON} (Fig. 2b). For the absolute ON-state current values, when the width increases, I_{ON} increases linearly in narrower PNR FETs, while it rises sub-linearly in wider PNRs. The shape of the I_{ON} - W curve in Fig. 2a, in the case of ideal contacts, results in a non-trivial width-dependence of the normalized I_{ON} in Fig. 2b that exhibits a local minimum for $W = 3.43$ nm. In the case of metal contacts, normalized I_{ON} seems to saturate at about 0.5 mA/µm for PNR widths above 1.5 nm. This behavior is expected since the absolute I_{ON} in Fig. 2a increases sub-linearly when the PNR width increases.

These results show that the inclusion of metal contacts reduces the current in comparison to ideal contact regions, meaning that the usually assumed nanoribbon S/D regions significantly over-estimate FET current-driving capabilities. Metal contacts described with WBL indeed have a wide energy-band, allowing electron injection from contacts for the entire energy-band of the channel. However, the bandstructure of S/D regions is not identical to that of the channel region, which causes qualitative and quantitative changes. Namely, the shape of the allowed energy states changes considerably, and a non-unitary transmission through the channel is observed due to quantum interference that is possible in coherent transport. These effects are seen as oscillations in transmission and DOS and, moreover, metal contacts lead to increased DOS and transmission within the bandgap. This topic is not analyzed further in this work since the main conclusions are known from previous studies on graphene nanoribbons (GNRs) with non-ideal contacts [19]. Therefore, we can conclude that PNR FETs with metal contacts generally exhibit lower I_{ON}, higher I_{OFF}, and a significantly lower ON-OFF ratio as discussed in the next paragraph.

Figure 3 reports I_{ON} vs. ON-OFF current ratio for PNR FETs with ideal and metal contacts. Generally, PNR devices with ideal nanoribbon S/D regions exhibit greater I_{ON} and ON-OFF current ratio, with the latter being in excess of 10^6. The inserted literature data for other contending 2D-material-based MOSFETs [9], [20]–[22] shows that PNR FETs with ideal contact regions exhibit similar performance as germanene FETs or GNR FETs. Moreover, PNR FETs with ideal contacts show higher ON-OFF current ratio than arsenene, antimonene and silicene FETs. Even metal-contact PNR devices fulfill IRDS requirement for the ON-OFF ratio ($> 2 \cdot 10^5$), however, neither group of the examined PNR FETs satisfies the I_{ON} requirement (1.95 mA/µm) since the maximum obtained equals 1.85 mA/µm for the device with 4.41 nm-wide PNR.

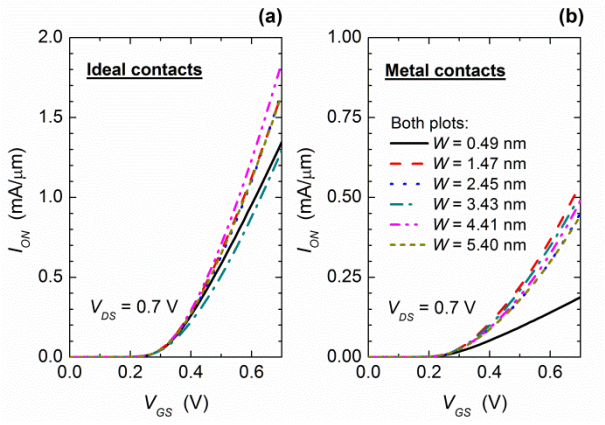

Fig. 1. Transfer characteristics of PNR MOSFETs at $V_{DS} = 0.7$ V for (a) ideal nanoribbon contacts and (b) metal contacts in the wide-band limit. Including metal contacts reduces I_{ON} by up to 72% (equiv. to $R_{SD} = 1470$ Ωµm).

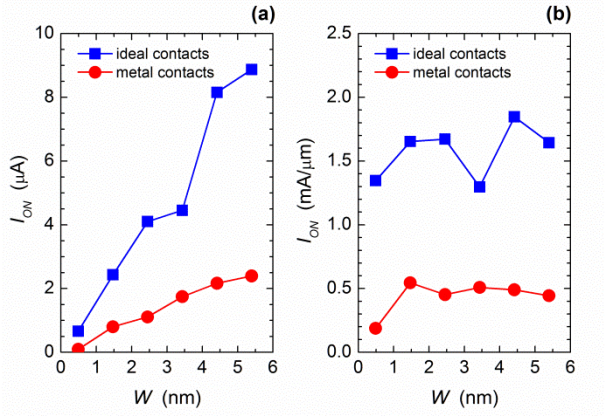

Fig. 2. ON-state current versus PNR width with current (a) expressed in absolute units and (b) normalized by PNR width. Absolute I_{ON} decreases monotonically while normalized I_{ON} exhibits local minima/maxima.

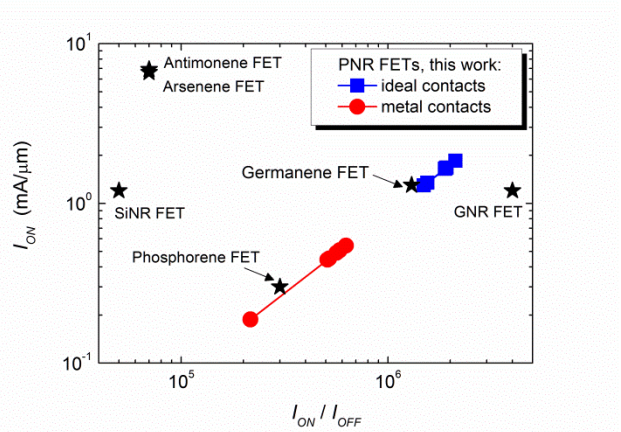

Fig. 3. ON-state current vs. ON-OFF current ratio for PNR MOSFETs with ideal and metal contacts. Data for other 2D material FETs from literature is inserted for comparison.

In addition to current-related FOMs, we investigate the intrinsic delay time (τ), as an intrinsic limit to switching speed, and power-delay product (PDP), which gives the limit of dynamic power dissipation. The PDP vs. delay plot is

reported in Fig. 4 for PNRs with ideal and metal contacts, with inserted literature data for other 2D material FETs. We observe that PDP generally increases with increasing delay, and while both PNR FET groups exhibit similar switching energies of up to 0.04 fJ/μm, delay time differs significantly. In the case of ideal contacts, delay reaches up to only 31 fs, while the lower driving currents in devices with metal contacts lead to much higher delay of up to 129 fs. This increase means that significantly lower switching speeds are achievable when more realistic metal contacts are considered. In terms of PDP (switching energy), both PNR FET structures are comparable to germanene FETs and outperform MoS_2 FETs and even antimonene/arsenene FETs. As for the delay (switching speed), PNR FET with metal contacts are comparable to all the examined alternatives, while ideal-contact PNR devices outperform all others.

As discussed previously, PNR FETs with metal contacts that are modeled with the WBL approximation exhibit I_{ON} values that on average reach 28% of the ballistic limit in devices with ideal contacts. While the contact parameters presented in the methodology section seem reasonable, the observed I_{ON} decrease corresponds to total contact/series resistance (R_{SD}) of 1470 Ωμm. While this value is comparable to experimentally measured resistance in phosphorene FETs [8], it is way above IRDS requirements. Therefore, we apply the required maximum R_{SD} = 275 Ωμm according to IRDS at N3 on device characteristics obtained numerically for PNR FETs with ideal contacts. Figure 5 reports I_{ON} for various PNR widths when R_{SD} = 275 Ωμm is assumed, and moreover reports I_{ON} dependence on transport ballisticity. This plot allows us to determine ballisticity values needed to fulfill the IRDS targets for the ON-state current that equals 0.91 mA/μm with non-zero R_{SD}. We find that ballisticity levels needed range from 50% to 70%, depending on the nanoribbon width, in order to attain the IRDS goal.

The obtained ballisticity limits seem reasonable and achievable in nanodevices. For example, recent theoretical/simulation work on 10.5 nm-long and wide-phosphorene (not nanoribbons) MOSFETs demonstrated 88-93% ballisticity when full-band electron-phonon scattering is included in the simulations. In order to provide an initial assessment of the ballisticity limit in the case of PNR FETs, we perform dissipative quantum transport simulations for the ON-state with optical phonons (OPs) included. Here, 4.4 nm-wide PNR is described with a single-band effective-mass Hamiltonian, for the sake of simplicity and numerical efficiency. Electron-phonon scattering was included using the self-consistent Born approximation [23], [24], real part of the scattering self-energy was neglected and only diagonal elements are retained. Optical phonon energy of E_{OP} = 32 meV and OP coupling strength of D_{OP} = 170 eV/nm is used in the simulations [10]. Figure 6 shows electron current density in the ON-state for the 4.4 nm-wide PNR FET in the case of coherent ballistic (Fig. 6a) and non-coherent dissipative (Fig. 6b) transport. The inclusion of OPs causes a small change in the current spectrum, with the distribution on the drain side being somewhat wider and with a lower average carrier energy, and no change in the electrostatic profile. For this device, I_{ON} in the dissipative case reaches 82% of the coherent ballistic limit, which means that PNR FETs are expected to fulfill IRDS goals for all the examined PNR widths if R_{SD} can be lowered to 275 Ωμm

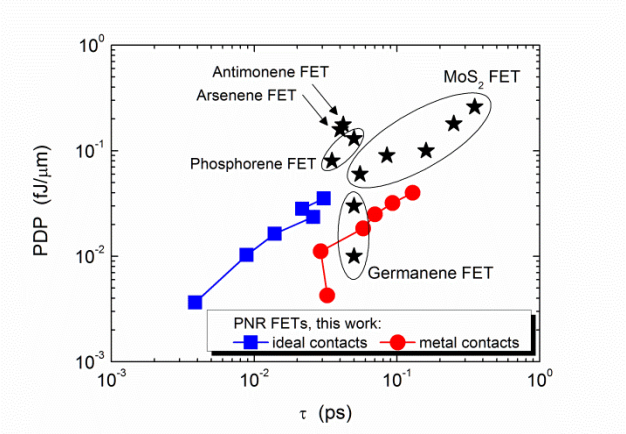

Fig. 4. Power-delay product vs. intrinsic delay time in PNR MOSFETs compared to other reported results from the literature. PNR devices outperform MoS_2, antimonene, arsenene and phosphorene FETs.

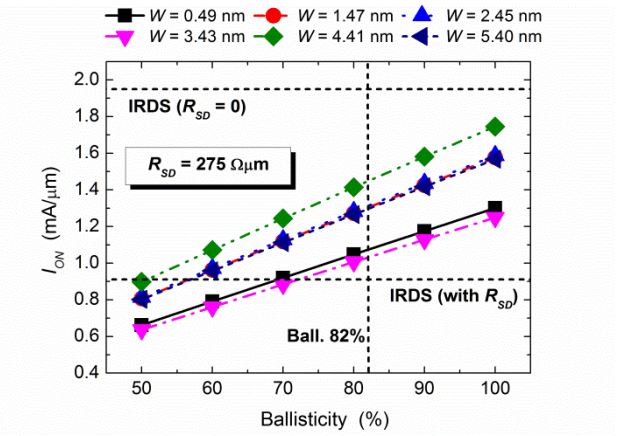

Fig. 5. Impact of ballisticity on the ON-state current in PNR MOSFETs with included parasitic series resistance of S/D regions (R_{SD} = 275 Ωμm).

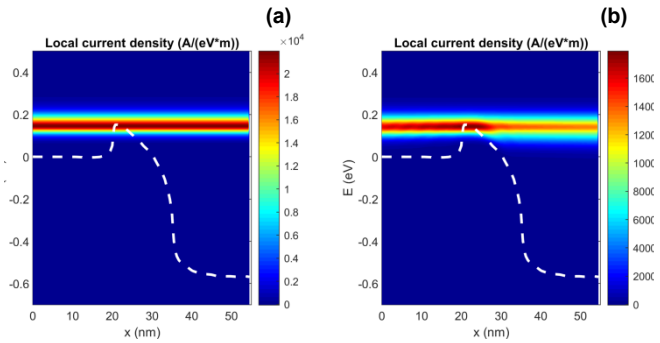

Fig. 6. Position and energy-resolved ON-state current density in 4.4 nm-wide PNR MOSFETs under (a) coherent ballistic transport and (b) dissipative transport with optical phonon scattering (E_{OP} = 32 meV, D_{OP} = 170 eV/nm). In the dissipative case, the ON-state current reaches 82% of the ballistic limit.

(see discussion related to Fig. 5). We note that including more subbands, or introducing additional scattering mechanisms such as acoustic phonon or lattice defect

scattering, would reduce the ballisticity additionally, but the extent of that decrease is beyond the scope of this work.

IV. Conclusion

Several important figures-of-merit of PNR MOSFETs with 15 nm-long channel are analyzed using atomistic NEGF simulations coupled with ToB model. The focus is on exploring the impact of metal contacts in WBL approximation, series resistance, ballisticity and nanoribbon width scaling on the performance of PNR transistors. We find that including realistically described metal contacts in NEGF simulations decreases I_{ON} by up to 72%, which is equivalent to R_{SD} of 1470 Ωμm. While this R_{SD} value agrees with experiments, it is more than 5× larger than the resistance limit set by IRDS. By including the IRDS-required series resistance, we find that PNR FETs should operate at 50% to 70% of the ballistic limit in order to attain IRDS goal for I_{ON}. Dissipative simulation with optical phonons reveals ballisticity of 82% in the ON-state. If good metal-phosphorene contacts are engineered such that R_{SD} can be lowered to about 270 Ωμm, PNR FETs with sub-5 nm-wide nanoribbon channels would be promising to fulfill IRDS-HP requirements at "3 nm" logic technology node.

References

[1] H. Liu *et al.*, "Phosphorene: An Unexplored 2D Semiconductor with a High Hole Mobility," *ACS Nano*, vol. 8, no. 4, pp. 4033–4041, Apr. 2014, doi: 10.1021/nn501226z.

[2] S. Das, W. Zhang, M. Demarteau, A. Hoffmann, M. Dubey, and A. Roelofs, "Tunable Transport Gap in Phosphorene," *Nano Letters*, vol. 14, no. 10, pp. 5733–5739, Oct. 2014, doi: 10.1021/nl5025535.

[3] A. Szabo, R. Rhyner, H. Carrillo-Nunez, and M. Luisier, "Phonon-limited performance of single-layer, single-gate black phosphorus n- and p-type field-effect transistors," in *2015 IEEE International Electron Devices Meeting (IEDM)*, Dec. 2015, pp. 297–300, doi: 10.1109/IEDM.2015.7409680.

[4] M. Poljak and T. Suligoj, "Immunity of electronic and transport properties of phosphorene nanoribbons to edge defects," *Nano Research*, vol. 9, no. 6, pp. 1723–1734, Jun. 2016, doi: 10.1007/s12274-016-1066-1.

[5] M. Poljak, "Electron Mobility in Defective Nanoribbons of Monoelemental 2D Materials," *IEEE Electron Device Letters*, vol. 41, no. 1, pp. 151–154, Jan. 2020, doi: 10.1109/LED.2019.2952661.

[6] S. Das, M. Demarteau, and A. Roelofs, "Ambipolar Phosphorene Field Effect Transistor," *ACS Nano*, vol. 8, no. 11, pp. 11730–11738, Nov. 2014, doi: 10.1021/nn505868h.

[7] Y. Du, H. Liu, Y. Deng, and P. D. Ye, "Device Perspective for Black Phosphorus Field-Effect Transistors: Contact Resistance, Ambipolar Behavior, and Scaling," *ACS Nano*, vol. 8, no. 10, pp. 10035–10042, Oct. 2014, doi: 10.1021/nn502553m.

[8] N. Haratipour, M. C. Robbins, and S. J. Koester, "Black Phosphorus p-MOSFETs With 7-nm HfO2 Gate Dielectric and Low Contact Resistance," *IEEE Electron Device Letters*, vol. 36, no. 4, pp. 411–413, Apr. 2015, doi: 10.1109/LED.2015.2407195.

[9] F. Liu, Y. Wang, X. Liu, J. Wang, and H. Guo, "Ballistic Transport in Monolayer Black Phosphorus Transistors," *IEEE Transactions on Electron Devices*, vol. 61, no. 11, pp. 3871–3876, Nov. 2014, doi: 10.1109/TED.2014.2353213.

[10] A. Afzalian and G. Pourtois, "ATOMOS: An ATOmistic MOdelling Solver for Dissipative DFT Transport in Ultra-Scaled HfS2 and Black Phosphorus MOSFETs," in *Proc. SISPAD*, 2019, pp. 199–202.

[11] E. Taghizadeh Sisakht, M. H. Zare, and F. Fazileh, "Scaling laws of band gaps of phosphorene nanoribbons: A tight-binding calculation," *Phys. Rev. B*, vol. 91, no. 8, p. 085409, Feb. 2015, doi: 10.1103/PhysRevB.91.085409.

[12] M. Poljak and T. Suligoj, "The Potential of Phosphorene Nanoribbons as Channel Material for Ultrascaled Transistors," *IEEE Trans. Electron Devices*, vol. 65, no. 1, pp. 290–294, Jan. 2018, doi: 10.1109/TED.2017.2771345.

[13] A. N. Rudenko and M. I. Katsnelson, "Quasiparticle band structure and tight-binding model for single- and bilayer black phosphorus," *Phys. Rev. B*, vol. 89, no. 20, p. 201408, May 2014, doi: 10.1103/PhysRevB.89.201408.

[14] M. P. L. Sancho, J. M. L. Sancho, J. M. L. Sancho, and J. Rubio, "Highly convergent schemes for the calculation of bulk and surface Green functions," *J. Phys. F: Met. Phys.*, vol. 15, no. 4, p. 851, 1985, doi: 10.1088/0305-4608/15/4/009.

[15] D. Kienle and A. W. Ghosh, "Atomistic Modeling of Metal-Nanotube Contacts," *J Comput Electron*, vol. 4, no. 1, pp. 97–100, Apr. 2005, doi: 10.1007/s10825-005-7116-7.

[16] A. Rahman, Jing Guo, S. Datta, and M. S. Lundstrom, "Theory of ballistic nanotransistors," *IEEE Transactions on Electron Devices*, vol. 50, no. 9, pp. 1853–1864, Sep. 2003, doi: 10.1109/TED.2003.815366.

[17] S. Kaneko, H. Tsuchiya, Y. Kamakura, N. Mori, and M. Ogawa, "Theoretical performance estimation of silicene, germanene, and graphene nanoribbon field-effect transistors under ballistic transport," *Appl. Phys. Express*, vol. 7, no. 3, p. 035102, Mar. 2014, doi: 10.7567/APEX.7.035102.

[18] "IEEE International Roadmap for Devices and Systems (IRDS), 2019 Update." https://irds.ieee.org/.

[19] G. Liang, N. Neophytou, M. S. Lundstrom, and D. E. Nikonov, "Ballistic graphene nanoribbon metal-oxide-semiconductor field-effect transistors: A full real-space quantum transport simulation," *Journal of Applied Physics*, vol. 102, no. 5, p. 054307, Sep. 2007, doi: 10.1063/1.2775917.

[20] G. Fiori and G. Iannaccone, "Simulation of Graphene Nanoribbon Field-Effect Transistors," *IEEE Electron Device Letters*, vol. 28, no. 8, pp. 760–762, Aug. 2007, doi: 10.1109/LED.2007.901680.

[21] G. Pizzi, M. Gibertini, E. Dib, N. Marzari, G. Iannaccone, and G. Fiori, "Performance of arsenene and antimonene double-gate MOSFETs from first principles," *Nature Communications*, vol. 7, p. 12585, Aug. 2016.

[22] Y. Zhao, A. AlMutairi, and Y. Yoon, "Assessment of Germanane Field-Effect Transistors for CMOS Technology," *IEEE Electron Device Letters*, vol. 38, no. 12, pp. 1743–1746, Dec. 2017, doi: 10.1109/LED.2017.2763120.

[23] M. Luisier, "Quantum transport beyond the effective mass approximation," Doctoral Thesis, ETH Zurich, 2007.

[24] M. Pourfath, *The Non-Equilibrium Green's Function Method for Nanoscale Device Simulation*. Wien: Springer-Verlag, 2014.